Available online at www.sciencedirect.com

ScienceDirect

Procedia Structural Integrity 24 (2019) 28–39

Structural Integrity Procedia

www.elsevier.com/locate/procedia

AIAS 2019 International Conference on Stress Analysis

Two-Dimensional Discrete Model for Buckling of Helical Springs

Francesco De Crescenzo[a]*, Pietro Salvini[a]

[a]*Department of Enterpirese Engineering, University of Rome "Tor Vergata", via del Politecnico, 1 00133, Rome, Italy*

Abstract

The classical theory of helical spring instability is based on the buckling of an equivalent column. Alternatively, more advanced methods are found in literature, involving the numerical solution of the displacement field of the helical wire. Those approaches turn challenging when the helix is non-uniform or there is the need to take into account contact between coils. In this work, the buckling behaviour of uniform helix springs is investigated using a 2D model with lumped stiffness, so that it can be compared to the previous modelling techniques. The aim is, after validation, to adopt the proposed technique to non-uniform springs. The spring is modelled as a planar structure made of rigid rods connected by nonlinear elastic hinges. Each rod thus represents half a coil, and each hinge lumps the stiffness of the adjacent two-quarters of a coil. Because of nonlinearity, the equilibrium is solved for incremental loads. At each step, the stability of the spring is evaluated from the eigenvalues of the tangent stiffness (geometric end elastic contributions).

Keywords: Helical Springs; Nonlinear Buckling, Discrete modeling

* Corresponding author. Tel.: +39.06.7259.7140; fax: +39.06.7259.7140.
E-mail address: francesco.de.crescenzo@uniroma2.it

10.1016/j.prostr.2020.02.003

1. Introduction

1.1. Applications

The functionality of many mechanical systems depends on the capability of helical springs to absorb, store and release elastic energy. Just mentioning few examples, helical springs are key components in combustion engine distribution systems, vehicle suspensions, vibration insulating platforms, and in the actuation of safety mechanisms.

In all previous situations, helical springs are mostly loaded with an axial compressive force along their centreline, which may induce buckling if the spring is not properly designed. Moreover, axial loads lower the frequencies of lateral vibration modes, which may evidence unexpected resonances. In both cases, the spring may not operate at the design conditions anymore and this may compromise the performance, or even the integrity, of the whole system. The two phenomena, static instability and lowering of frequencies, are related and have often been studied together Kobelev (2014), Yildrim (2009).

Nomenclature

E	Young's modulus of elasticity, N/m^2
G	shear modulus, N/m^2
I	moment of inertia of wire cross-section, m^4
J	polar moment of inertia of wire cross-section, m^4
n	number of coils
x	generalized degree of freedom
α	helix angle, rad
ν	Poisson's ratio

1.2. Haringx's model

The classical solution to the buckling of helical springs is that of Haringx (1948). He derived a simple model to predict instability, based on the buckling of an equivalent shearable column. The spring is modelled as an elastic column whose section properties depend on the deformed length in such a way that axial, bending, and shearing characteristics of the whole column are constant during compression. With this assumption, Haringx obtained a closed formula for buckling prediction, where the critical deflection of the spring is a function of spring slenderness only. This solution is very useful in early design stages and in good agreement with experimental results, especially when the number of coils is large, helix pitch is small and the wire is thin with respect to the coil radius. Haringx also showed the range of validity of his results giving an approximated solution of the elastica of the wire. He found the “auxiliary” helix that represents the deformed spring: this accounts for the effects of bending and torsion induced in the wire by the axial load. Finally, he considered small displacements and small rotations around the compressed state to check for instability.

1.3. Models based on helical wire elastica

In the following fifty years the problem was investigated by several authors, with the aim to obtain a better solution valid for springs not covered by Haringx model. The common approach recalls Haringx’s auxiliary helix and accounts of the differential equations governing the dynamics of the deformed wire. A numerical method is used for the search of eigenfrequencies, corresponding to a given axial load. Furthermore, the buckling condition (static response) corresponds to the load at *0* frequency, where the stiffness vanishes. The works differ for both the equation adopted (rotary inertia, shear deformation, prestress terms, …) and for the numerical method used to solve the system, which turns out to be made of 12 differential equations in 12 unknowns. Pearson (1982), Becker et al. (1992), Chassie et al. (1996) and Yildrim (2009) used Transfer Matrix Method (TMM); Mottershead (1982) also developed a helical Finite Element (FE).

Both approaches are really effective. In particular, TMM gives the exact solution for a uniform helix at a very low computational cost. Mottershead's FE performs well and requires much coarser mesh than a standard FE analysis with beam elements. However, the effectiveness of those methods reduces when the helix is non-uniform since a more advanced formulation or a finer mesh is needed, Yildrim (1997). Furthermore, if coils clash and friction between the coils is to be taken into account, Wu et al. (1998), the implementation of TMM and helical FE methods becomes challenging. For this reason, the authors developed a 2D lumped model for helical springs buckling prediction, intending to extend it to non-uniform helices and to account possible coil contacts.

2. Model geometry and governing equations

The proposed model is a planar structure made of rigid rods coupled by elastic hinges (Fig. 1).The rods are rigid and the stiffness of the hinges is deformation-dependent. Each elastic hinge lumps the stiffness of the adjacent two-quarter of a coil. The lumped model must have the same nonlinear axial load-deflection curve of the real spring. Moreover, to account for coil shearing, a linear spring is placed between the ends of adjacent rods, oriented along the bisector of the corresponding angle. Thus, each square in Fig.1 reacts with a torque to variation in relative angle between the rods, and with a sliding force against relative translations along angle bisector. First rod (link *1*) and the last one (link $2n+2$) are dummy but needed to represent the clamped condition at helix ends.

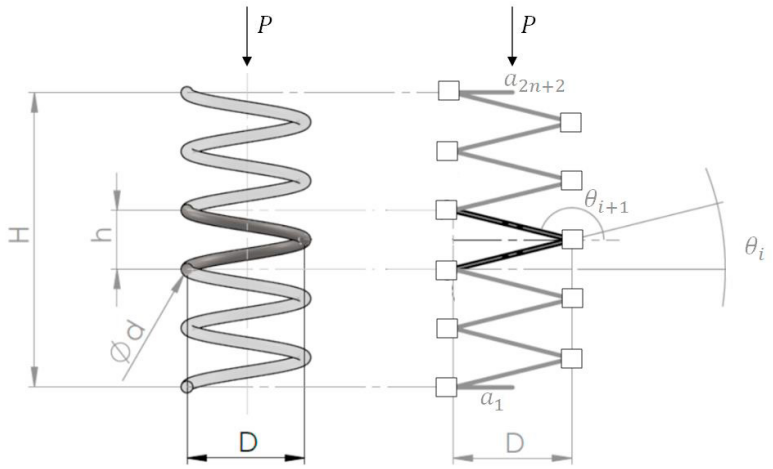

Fig. 1. General representation of helical spring and its corresponding 2D discrete model.

The configuration of the links is given by the vector of rotations $\boldsymbol{\theta} = \{\theta_1, \theta_2, \dots, \theta_{2n+2}\}^T$ and the vector of translations $\boldsymbol{u} = \{u_1, u_2, \dots, u_{2n+1}\}^T$, where n is the number of coils. The total number of degrees of freedom is thus $4n+3$. θ_i represents the angle of rod i with respect to the horizontal line, u_i represents the translation of rod $i+1$ with respect to rod i. It follows that the total height of the spring is:

$$H = \sum_{i=1}^{2n+2} a_i \sin\theta_i + \sum_{k=1}^{2n+1} u_k \sin b_k \tag{1}$$

where a_i is the length of the rod and b_k is the angle of the bisector with respect to the horizontal line:

$$b_k = \frac{\theta_i + \theta_{i+1}}{2} - \frac{\pi}{2} \tag{2}$$

The potential of the load P compressing the spring is:

$$V_P = PH = P\left(\sum_{i=1}^{2n+2} a_i \sin\theta_i + \sum_{k=1}^{2n+1} u_k \sin b_k\right) \tag{3}$$

At any equilibrium point $\mathbf{x_0} = \{\boldsymbol{\theta_0}, \boldsymbol{u_0}\}^T$ the sum of elastic and load potential is stationary; thus, $grad(V_E + V_P) = \mathbf{0}$. This leads to the $2n+2$ equations describing the rotational equilibrium of the i_{th} rods and to $2n+1$ equations for the shearing of k_{th} linear spring:

$$\frac{\partial V_E}{\partial \theta_i} + \frac{\partial V_P}{\partial \theta_i} = 0 \qquad i = 1,\ldots,2n+2 \tag{4}$$

$$\frac{\partial V_E}{\partial u_k} + \frac{\partial V_P}{\partial u_k} = 0 \qquad k = 1,\ldots,2n+1 \tag{5}$$

If an incremental load ΔP is applied to the structure, the gradient of corresponding potential $V_{P+\Delta P}$ will not be balanced by the elastic forces anymore, however it is still reasonable to look for equilibrium point near $\boldsymbol{x_0}$ expanding terms in the previous equations:

$$\frac{\partial V_E}{\partial x_i}_{|\boldsymbol{x}=\boldsymbol{x_0}} + \sum_{j=1}^{4n+3} \frac{\partial^2 V_E}{\partial x_j \partial x_i}_{|\boldsymbol{x}=\boldsymbol{x_0}} \Delta x_j + \frac{\partial V_P}{\partial x_i}_{|\boldsymbol{x}=\boldsymbol{x_0}} + \sum_{j=1}^{4n+3} \frac{\partial^2 V_P}{\partial x_j \partial x_i}_{|\boldsymbol{x}=\boldsymbol{x_0}} \Delta x_j + \frac{\partial V_{\Delta P}}{\partial x_i}_{|\boldsymbol{x}=\boldsymbol{x_0}} = 0 \qquad i = 1,2,\ldots 4n+3 \tag{6}$$

On the assumption that $\boldsymbol{x_0}$was an equilibrium point associated to load P, it gives:

$$\sum_{j=1}^{4n+3} \frac{\partial^2 V_E}{\partial x_j \partial x_i} \Delta x_j + \sum_{j=1}^{4n+3} \frac{\partial^2 V_P}{\partial x_j \partial x_i} \Delta x_j + \frac{\partial V_{\Delta P}}{\partial x_i} = 0 \qquad i = 1,2,\ldots 4n+3 \tag{7}$$

Eq.(7) can be written in matrix form as:

$$(\boldsymbol{K}_e + \boldsymbol{K}_g)\boldsymbol{\Delta x} = \boldsymbol{\Delta F} \tag{8}$$

where the sum $(\boldsymbol{K}_e + \boldsymbol{K}_g)$ is the tangent stiffness, considering elastic and geometric contributions, $\boldsymbol{\Delta F}$ is the vector of external loads increment and $\boldsymbol{\Delta x}$ is the corresponding incremental displacement. Since eq.(8) is only a linear approximation of the incremental equilibrium, an iterative procedure must be implemented in order to find a solution within a prescribed tolerance.

3. Derivation of stiffness parameters

3.1. Load potential and geometric stiffness matrix

Geometric stiffness terms are obtained performing the second partial derivative of load potential in eq.(3). For easiness of writing, in the following the numbering of the degrees of freedom starts from 0 , $(b_0, u_0, b_{2n+2}, u_{2n+2}) \equiv 0$; thus avoiding the need of explicitly writing the expressions involving first and last rods. It is useful to separate the contribution of pure rotation, pure shearing and rotation-shearing coupling terms.

Derivation of terms in the rotation-to-rotation geometric stiffness block ${}^{\theta\theta}K_{g_{ij}}$ is straightforward. Starting from the potential, the calculation of the second derivatives gives:

$${}^{\theta\theta}K_{g_{ij}} = \frac{\partial^2 V_P}{\partial \theta_j \partial \theta_i} = P\left(-a_i \sin\theta_j - \frac{1}{4} u_{i-1} \sin b_{j-1} - \frac{1}{4} u_i \sin b_j\right)\delta_{ij} \tag{9}$$

where δ_{ij} is the Kronecker delta, thus ${}^{\theta\theta}K_{g_{ij}}$ is a diagonal matrix.

Rotation and shearing are coupled, in fact the shearing effect of the load depends on the bisectors, which are a function of the angles of adjacent rods. Non-zero terms are of the rotation-to-shearing block are:

$$ {}^{\theta u}K_{g_{ik}} = \frac{\partial^2 V_P}{\partial u_k \partial \theta_i} = \frac{1}{2} P \cos b_k = \quad {}^{u\theta}K_{g_{ki}} \tag{10}$$

with $k = i - 1 \; and \; i$, considering $k \neq 0$.

As the load is vertical, there is no pure shearing geometric effect:

$$ {}^{uu}K_{g_{kj}} = \frac{\partial^2 V_{P+\Delta P}}{\partial u_j \partial u_k} = 0 \tag{11}$$

for all k, j.

Ordering the degrees of freedom the complete geometric stiffness is obtained:

$$ \boldsymbol{K_g} = \begin{bmatrix} {}^{\boldsymbol{\theta\theta}}\boldsymbol{K_g} & {}^{\boldsymbol{\theta u}}\boldsymbol{K_g} \\ {}^{\boldsymbol{u\theta}}\boldsymbol{K_g} & {}^{\boldsymbol{uu}}\boldsymbol{K_g} \end{bmatrix} \tag{12}$$

3.2. Elastic deformation energy

Elastic stiffness can be computed from the increment of elastic energy in a single coil under compression, as shown in Fig. 2. The fundamental assumptions are the followings:

- each hinge lumps the stiffness of a two-quarters of a coil
- two-quarter-coil compression is related to the angle between adjacent links

When the compression increases of an infinitesimal dh, the corresponding increment of elastic energy is

$$ \Delta E_H = \frac{1}{2} K_H dh^2 \tag{13}$$

where K_H is the tangent stiffness of the coil, and will be derived in the next section. In the 2D lumped coil, the elastic energy is stored by the two torsion springs k_t subjected to angular deflection $d\beta$:

$$ \Delta E_t = 2 \frac{1}{2} k_t d\beta^2 \tag{14}$$

The kinematic constraint is:

$$ dh = 2a \cos\theta \, d\theta \tag{15}$$

where $d\theta$ is the variation in rod slope and $d\beta = 2d\theta$ for symmetry. The value of K_t is found by equating the energy of the 2D model to that of the coil:

$$ \Delta E_H = \frac{1}{2} K_H (2a \cos\theta \, d\theta)^2 = k_t (2d\theta)^2 = \Delta E_t \tag{16}$$

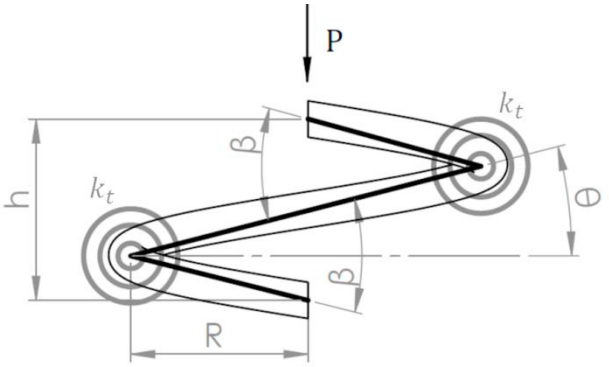

Fig. 2. Two springs, each one lumping two-quarters of a coil.

which gives:

$$k_t = \frac{1}{2} K_H a^2 \cos\theta^2 \tag{17}$$

3.3. Load-deflection characteristics of single coil

Axial force/deflection characteristics are derived following Wahl (1963). Shear and axial deformability of the wires are neglected, thus variation in radius and pitch can be related to wire curvature and torsion. Curvature and torsion of a cylindrical helix with radius R and angle α are:

$$\kappa = \frac{\cos^2\alpha}{R} \tag{18}$$

$$\tau = \frac{\cos\alpha \sin\alpha}{R} \tag{19}$$

For large spring index ($C = \frac{D}{d} \gg 1$) bending and torsional moments can be related to the change in curvature and torsion Wahl (1963):

$$M_b = EI \left(\frac{\cos^2\alpha}{R} - \frac{\cos^2\alpha_0}{R_0} \right) \tag{20}$$

$$M_t = GJ \left(\frac{\cos\alpha \sin\alpha}{R} - \frac{\cos\alpha_0 \sin\alpha_0}{R_0} \right) \tag{21}$$

Bending and torsion moments due to an axial load acting along helix centreline are:

$$M_b = PR \sin\alpha \tag{22}$$

$$M_t = PR \cos\alpha \tag{23}$$

Furthermore, the wire is inextensible and total length is preserved:

$$n \frac{2\pi R}{\cos\alpha} = n_0 \frac{2\pi R_0}{\cos\alpha_0} \tag{24}$$

It is convenient to assign a value to the helix angle and then to compute the corresponding radius and load. By this way, it is possible to table loads against deflection and to compute the tangent characteristic of the coil using central difference

$$R = R_0 \left[\frac{1}{\cos^2 \alpha} \left(\sin \alpha_0 \cos \alpha_0 \tan \alpha + \frac{E}{2G} \cos^2 \alpha_0 \right) \left(\frac{E}{2G} + \tan^2 \alpha \right) \right] \tag{25}$$

$$P = \frac{GJ}{R \cos \alpha} \left(\frac{\sin \alpha \cos \alpha}{R} - \frac{\sin \alpha_0 \cos \alpha_0}{R_0} \right) \tag{26}$$

$$\delta = -\frac{2\pi R_0 n_0}{\cos \alpha_0} (\sin \alpha - \sin \alpha_0) \tag{27}$$

Finally, tangent stiffness of the spring is given by:

$$K_h = \frac{\partial P}{\partial \delta} \tag{28}$$

3.4. Coil shearing characteristics

In the 2D discrete model, shearing of coils is lumped in two springs for each coil. In Fig.3a this is obtained with a full spring k_s that lumps two-quarters of coil and with two half-springs $2k_s$, that lump a quarter of coil each. The simplest model of coil shearing is the one used by Haringx in his work on spring buckling (Fig. 3b). The coil is projected on a plane perpendicular to helical axis, resulting in an open ring. One end of the ring is clumped and a radial force Q is applied to the other. A bending moment M' is here also applied to the free end, in order to hold it against rotation.

The bending moment along the wire and deformation energy are then:

$$M = M' + QR \sin \phi \tag{29}$$

$$U = \frac{1}{2} \int_0^{2\pi R} \frac{M^2}{EI} ds = \frac{1}{2} \int_0^{2\pi} \frac{M^2}{EI} R d\phi \tag{30}$$

and the integration gives:

$$U = \frac{M'^2 R\pi}{EI} + \frac{Q^2 R^3 \pi}{2EI} \tag{31}$$

where it is evident that the force Q is not inducing any rotation of the free end so that $M' = 0$. The radial displacement is found applying Castigliano's theorem:

$$q = \frac{\partial U}{\partial Q} = \frac{QR^3\pi}{EI} \tag{32}$$

Shearing stiffness of the coil is then:

$$K_Q = \frac{Q}{x} = \frac{EI}{R^3 \pi} \tag{33}$$

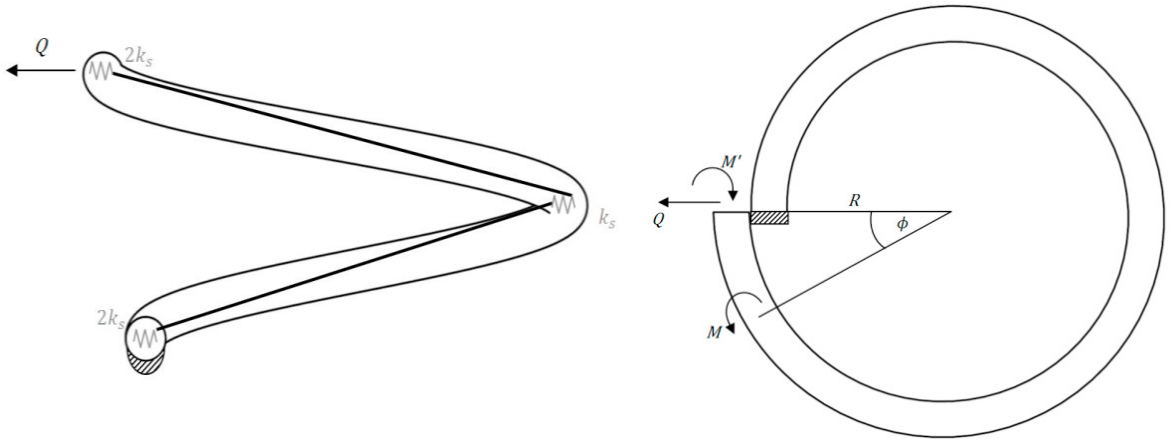

(a) (b)

Fig. 3. Shearing of a coil: a) 2D lumped model and b) simple model for stiffness estimation

and for a wire of solid circle cross-section it is:

$$K_Q = \frac{d^4 E}{8D^3} \tag{34}$$

Finally, in the 2D model, the shearing of a coil is obtained by the elongation of a total of two linear springs, whose stiffness must be thus two times that of the entire coil:

$$k_s = \frac{d^4 E}{4D^3} \tag{35}$$

3.5. Elastic stiffness matrix

In the same way as for the geometric stiffness, elastic stiffness matrix can be also divided into four blocks, depending on the degrees of freedom coupled by the terms: rotation-to-rotation, rotation-to-shearing, shearing-to-rotation and shearing to shearing.

Rotation-to-rotation block is easily obtained considering the forces needed to slightly rotate each rod while holding the others. When the i_{th}-link rotates of a quantity $d\theta_i$, a reaction torque will arise also on previous and following links. The elastic stiffness matrix is then tridiagonal with diagonal terms equal to the sum of the hinge stiffnesses at rod ends, and off-diagonal terms equal to minus the stiffness of previous and following hinge, respectively:

$$^{\theta\theta}\boldsymbol{K}_e = \begin{pmatrix} 2K_t & -2K_t & 0 & 0 & 0 & 0 & 0 & 0 \\ & 2K_t + K_t & -K_t & 0 & 0 & 0 & 0 & 0 \\ & & K_t + K_t & -K_t & 0 & 0 & 0 & 0 \\ & & & \ddots & -K_t & 0 & 0 & 0 \\ & & & & K_t + K_t & -K_t & 0 & 0 \\ & SYM & & & & \ddots & -K_t & 0 \\ & & & & & & K_t + 2K_t & -2K_t \\ & & & & & & & 2K_t \end{pmatrix} \tag{36}$$

The stiffness of first and last hinges is twice that of middle hinges, because they are lumping one quarter of coil.

The sharing-to-shearing block is diagonal, because the translational dofs already represents the relative shearing

at every hinge:

$$ {}^{uu}\boldsymbol{K_e} = \begin{pmatrix} 2K_s & 0 & 0 & 0 & 0 \\ 0 & K_s & \cdots & 0 & 0 \\ 0 & \vdots & \ddots & \vdots & 0 \\ 0 & 0 & \cdots & K_s & 0 \\ 0 & 0 & 0 & 0 & 2K_s \end{pmatrix} \tag{37} $$

Rotational and translational degrees of freedom are elastically decoupled, thus off-diagonal blocks of the complete elastic matrix are null. The global elastic stiffness matrix writes then:

$$ \boldsymbol{K_e} = \begin{bmatrix} {}^{\theta\theta}\boldsymbol{K_e} & \boldsymbol{0} \\ \boldsymbol{0} & {}^{uu}\boldsymbol{K_e} \end{bmatrix} \tag{38} $$

For clamped-clamped ends rotations of first and last rods are locked and the corresponding rows and columns are deleted.

4. Equilibrium and stability check

The solution procedure is similar to that of TMM: first, the equilibrium configuration corresponding to the "auxiliary helix" is found (only elastic stiffness used in the iterations), then the stability is checked using tangent stiffness (geometric and elastic terms). Buckling of the spring is evaluated from the behaviour of the eigenvalue of the corresponding buckling mode. In this study, the attention is focused on the second mode, according to the clamped-clamped boundary conditions.

Assuming that the solution is starting from an equilibrium configuration (which may be also the unloaded/undeformed state) and that the stiffness matrices are already computed, the steps of the solution are:

1. apply the incremental load $\boldsymbol{\Delta F_{ext} = \Delta P}$ and find the incremental displacement: $\boldsymbol{\Delta x^e = K_e \backslash \Delta F_e}$
2. update the displacements and the elastic stiffness matrix
3. compute the external and internal forces in the new configuration
4. compute the residuals $\boldsymbol{res = F_{ext} - F_{int}}$
5. if convergence criterion is not met $\boldsymbol{\Delta x^e = \Delta x^e + K_e \backslash res}$
6. iterate from step 2 until convergence is met
7. update elastic and geometric stiffness matrices
8. find the eigenvalues of $\left(\boldsymbol{K_g + K_e}\right)$
9. iterate from step 1 until the external load is fully applied

In case of a uniform helix, the auxiliary helix corresponding to a given axial load is known. Thus, it would be easier to avoid the equilibrium iterations and directly assemble the tangent stiffness matrix. However, since the aim of the model is to deal with non-uniform helix and coil contact, the iterative incremental procedure, being more generic, was preferred.

Table 1. Geometry of springs.

Spring no.	d (m)	D (m)	n (-)	H (m)	C (-)	ξ (-)
1	0.005	0.025	10	0.200	5	8
2	0.001	0.010	20	0.200	10	20
3	0.001	0.010	10	0.060	10	6
4	0.001	0.010	5	0.060	10	6
5	0.001	0.010	20	0.060	10	6
6	0.001	0.0075	10	0.080	7.5	10.7

The stability of the 2D model is assessed looking at the eigenvalue corresponding to the second buckling mode,

which is the one with clamped ends. The behaviour of eigenvalues and the shape of the buckling modes for spring no.5 are shown in Fig. 4a and Fig. 4b. The static buckling condition occurs when the eigenvalue crosses the zero value.

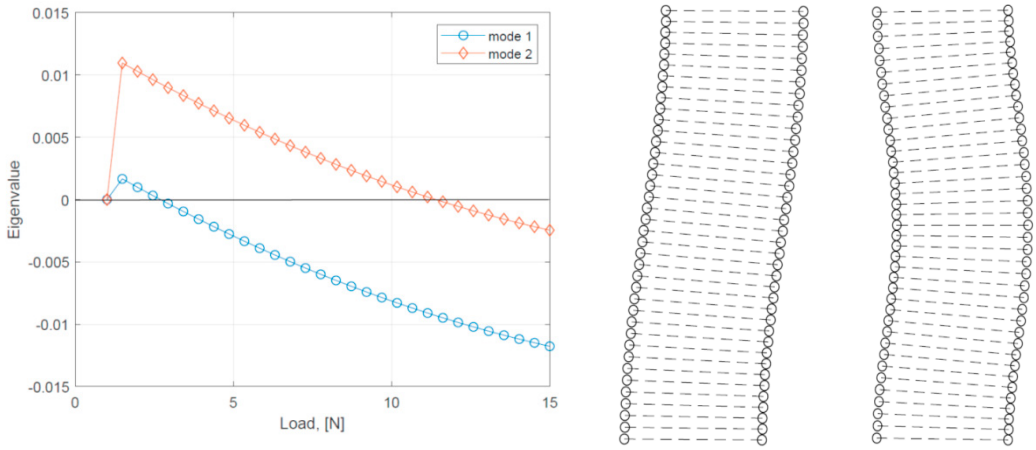

(a) (b)

Fig. 4. (a) Eigenvalues and (b) mode shapes of first and second buckling modes of spring no. 5.

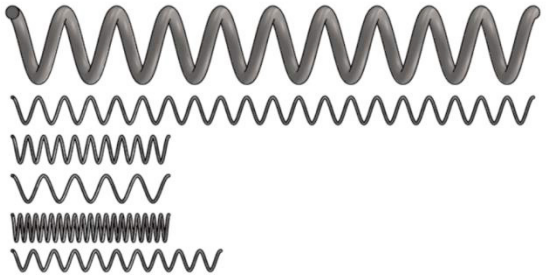

Fig. 5. Comparison of studied springs: spring 1 on top, spring 6 at bottom.

5. Results and discussion

5.1. Study cases

According to Haringx's theory, critical relative deflection at buckling is a function of spring slenderness only, defined se the ratio between spring height and coil diameter. Moreover, the role of coil shearing decreases with the slenderness and becomes almost negligible for slenderness ratio greater than 10. Keeping the slenderness constant, according to Haringx model, the number of coils should not affect the critical deflection. Nevertheless, both TMM results, as well as FE results, show a dependency with the number of coils. Six cases have been chosen in order to span a significant range of possibilities: slander to thick springs, with low to a large number of coils. All springs are made of steel and the following material properties were assumed: $E = 210\ GPa$, $\nu = 0.3$.

Spring 1 is moderately slender $\xi = 8$ and is characterized by a thick wire, resulting in a low coil to wire diameter ratio, $C = 5$. Spring 2 to 5 have the same wire diameter and index $C = 10$, so that shear deformation of the wire is negligible. Spring 2 is very slender $\xi = 20$, while the others are thick $\xi = 6$ (for Haringx theory, slenderness limit to instability, that is to say, no instability occurs, for clamped-clamped when $\xi < 5.24$). Springs 3,4 and 5 differ for the number of coils. Finally, spring 6 is moderately slender and has a smaller index than springs 3,4,5.

5.2. Comparison of the proposed model with respect to other methods

The results of the proposed method are compared with those obtained using Haringx classical theory, Transfer Matrix Method (TMM) and Finite Elements (FE) analysis on commercial software.

TMM is applied as described in Yildrim (2009), but the exponential matrix is computed using built-in function *expm()* and the compressed helix is computed neglecting shear and axial compression of the wire (same equations as those used for the coil characteristics in §3.3). Frequency terms are of course put to *0*.

FE analysis is performed on a commercial code. The structure has been modelled with iso-parametric beams with two nodes (120 elements each coil). Both ends are fully clamped, one is displaced parallel to spring axis towards the other. This means that there is some boundary effect in the FE element model, since the end coils cannot adjust their pitch to the "auxiliary helix". The constrained pitch behaves as an imperfection that triggers instability during the nonlinear static analysis in large displacements. However, this introduces a difference between FE element and other models, where the helix is "perfect", as can be seen in Spring no.4, characterized by the lowest number of coils, where FE buckling is less evident and it occurs much earlier than foreseen by the other methods.

Critical loads are listed in Tabel (2) and, with the former exception, are all within the 10% around the TMM solution, which may be considered the reference one. As a general trend, Haringx theory predicts greater critical loads than other methods, while the 2D model underestimating them. Fig. 6 shows the relative critical deflection versus springs slenderness ratio: all critical points are placed along the theoretical Haringx curve. For springs no.3,4,5 (the grouped values corresponding to slenderness *6* in the picture) it can be seen how the points move from the theoretical curve as the number of coils changes. It is interesting to highlight that the proposed 2D model is able to evidence the effect of the number of coils, regardless of slenderness invariance.

Table 2. Critical loads.

Spring no.	**Critical Load (N)**			
	Haringx	*TMM*	*FEM*	*2D*
1	1604	1559	1500	1410
2	2.87	2.76	2.74	2.56
3	25.3	25.0	23.9	23.0
4	50.5	49.6	39.2	47.8
5	12.6	12.6	12.5	11.5
6	20.1	19.2	18.8	17.8

6. Conclusions

A 2D discrete model with lumped stiffness is proposed to predict buckling of helical springs. The 2D model is made of rigid rods, elastic hinges lumping the axial and bending stiffness of the coils, and linear springs that account for coil shearing. This last plays an important role in the buckling of thick springs. Model parameters are identified using analytical models of coil deformation. The load is incrementally applied to the structure and the equilibrium is found iteratively.

The stability is checked at each load step from the eigenvalues of the tangent stiffness. The vanishing of the second eigenvalue (clamped-clamped ends) gives the critical load. The results are coherent with Haringx classical theory and with solutions of helix elastica by Transfer Matrix Method and Finite Element analysis. The 2D model shows a certain underestimate of the critical loads, but this may be corrected with parameters identification. In future works, the 2D-model will be usefully applied to non-uniform helices considering also the consequence of coil contacts. It is evident that in those scenarios a discrete lumped model may be a valid alternative to expansive FE analysis or complex semi-analytical methods.

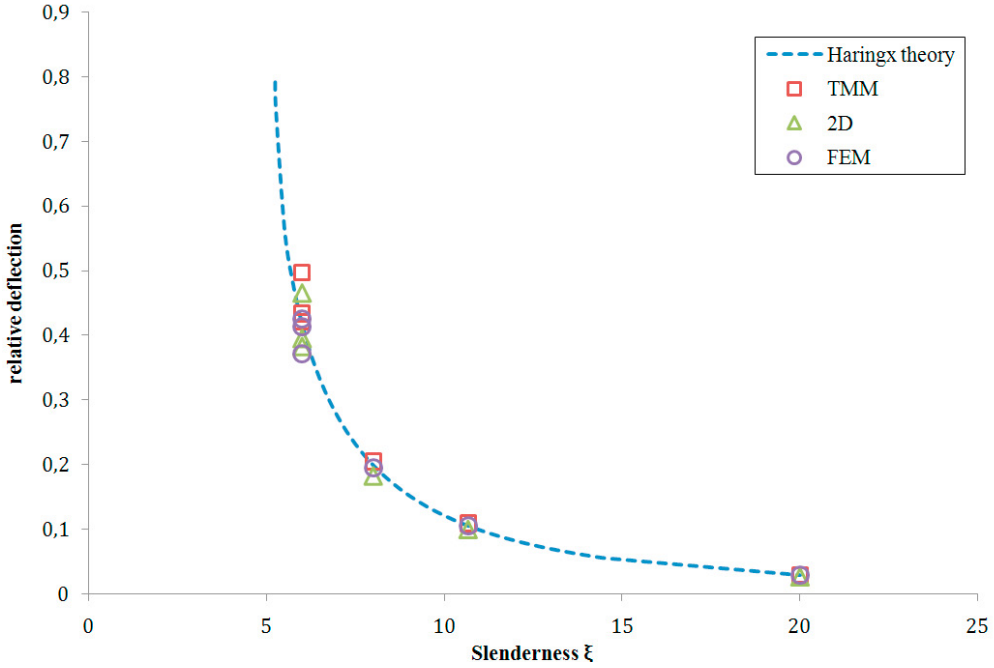

Fig. 6. Relative deflection at buckling against spring slenderness ratio.

References

Becker, L. E., & Cleghorn, W. L., 1992. On the buckling of helical compression springs. *International Journal of Mechanical Sciences* , Vol. 34, No. 4, pp.275-282.

Chassie, G. G., Becker, L. E., & Cleghorn, W. L., 1996. On the buckling of helcial springs under combined compression and torsion. *International Journal of Mechanical Sciences* , Vol. 39, No. 6, pp. 697-704.

Haringx, J. A., 1948. On highly compressible helical springs and rubber rods, and their application fo vibration-free mountings, part I. In *Philips Research Reports* (pp. 401-449). Eindhoven.

Kobelev, V., 2014. Effect of static axial compression on the natural frequencies of helical springs. *Multidiscipline Modeling in Materials and Structures* , Vol. 10, No. 3, pp. 379-398.

Mottershead, J. E.,1982. The large displacements and dynamic stability of springs using helical finite elements. *International Journal of Mechanical Sciences* , Vol. 24, No. 9, pp. 547-558.

Pearson, D., 1982. The transfer matrix method for the vibration of comrpessed helical springs. *Journal of mechanical engineering Sciences* , Vol.24, pp.163-171.

Wahl, A. M., 1963. *Mechanical springs.* New York: McGraw-Hill.

Wu, M. H., & Hsu, W. Y., 1998. Modelling the static and dynamic nehavior of a conical spring by considering the coil close and damping effect. *Journal of Sound and Vibration* , 17-28.

Yildrim, V., 1997. Natural frequencies of helical springs of arbitrary shape. *Journal of Sound and Vibration* , Vol. 204, No. 2, pp. 311-329.

Yildrim, V., 2009. Numerical buckling analysis of cylindrical helical coil springs in a dynamic manner. *International Journal of Engineering and Applied Sciences* , Vol. 1, pp. 20-32.